12^{th} International Conference on Fracture Mechanics of Concrete and Concrete Structures
FraMCoS-12
B.L.A. Pichler, Ch. Hellmich, P. Preinstorfer (Eds)

https://doi.org/10.21012/FC12.1283
MS18-2:1

FLUCTUATION-BASED DAMAGE MECHANICS: A STATISTICAL APPROACH TO FRACTURE IN CONCRETE

A. ATTIAS *, **F.-J. ULM** †

* Massachusetts Institute of Technology
77 Massachusetts Avenue, Cambridge, MA 02139, USA
e-mail: aattias@mit.edu

Massachusetts Institute of Technology
77 Massachusetts Avenue, Cambridge, MA 02139, USA
e-mail: ulm@mit.edu

Key words: Non-Local Fracture, Statistical Mechanics

Abstract. This study introduces a statistical mechanics framework for modeling fracture and damage processes in concrete materials, leveraging the semi-grand canonical ensemble. By conceptualizing fracture as a monolayer adsorption process and damage as a multi-layer adsorption phenomenon, the approach extends classical fracture mechanics through statistical observables and ensemble-based formulations. Through simulations on notched beams, the framework demonstrates key insights into the energy dissipation mechanisms underpinning fracture. Statistical observables, such as isosteric heats of adsorption, provide a robust method to predict fracture behavior without the need for experimental size-effect studies, while damage isotherms are highlighting the influence of configurational pressure on material degradation. The results emphasize the potential of this framework to enhance the predictive modeling of quasi-brittle materials, paving the way for applications in material design and structural engineering.

1 INTRODUCTION

Quasi-static fracture mechanics, as first formulated by Griffith in his seminal 1921 paper [1], describes fracture as an equilibrium process between two distinct material configurations under constant loading. In this framework, fracture propagation is governed by an irreversible material change, dictated by the energy released during incremental crack growth compared to a critical threshold: the critical energy release rate, $\mathcal{G}_c$. This foundational concept of dissipation rate catalyzed significant advancements in the field of fracture mechanics. Early theoretical approaches aimed to derive closed-form solutions for critical energy release rates across a wide range of fracture test [2–4]. Irwin's introduction of stress-intensity factors [5] further connected this global quantity to local material properties by decomposing fracture responses into the three distinct loading modes. More recently, the advent of variational formulations re-framed fracture mechanics as an energy-minimization problem [6–8], leveraging modern computational tools to simulate complex crack growth with high accuracy, including mixed-mode fracture [9], crack branching [10] and fracture of composite [11]. Despite these advancements, current methods share two significant shortcomings that limit their utility. First, they rely heavily on the concept of critical energy release rate, $\mathcal{G}_c$, which is experimentally costly and cumbersome to measure. Such measurements are test dependent and often require

size-effect studies across multiple specimens [12]. Second, existing methods are inherently deterministic, focusing on capturing the average response of a material under loading. This overlooks the inherent randomness and statistical nature of fracture phenomena. The work presented here revisits the concept of fracture through a statistical lens, building on Griffith's equilibrium and energy-driven framework. This statistical formalism is further extended to (non-local) damage processes and leverages statistical observables to better characterize failure processes.

2 FRACTURE AND DAMAGE IN THE SEMIGRAND ENSEMBLE

2.1 Fracture Mechanics as a monolayer adsorption process

To incorporate statistics into the fracture problem, we need to define an appropriate statistical ensemble. Consider a body $\Omega = \bigoplus_{k=1}^{N_0} \mathcal{P}_k$, subjected to a displacement loading x. The fracture state of each element $\mathcal{P}_k$ is characterized by a state variable $s^k \in \{0, 1\}$, where $s^k = 0$ represents the elastic state and $s^k = 1$ the fractured state. From a thermodynamic perspective, fracture is a surface process, and the system therefore does not exchange matter with its external bath. Thus, the total number of elements, N_0, is conserved, while their fracture state evolve as $N_0 = \sum_{k=1}^{N_0} \left[s^k N_b + (1 - s^k) N_e\right]$, where N_e and N_b are the numbers of elastic and broken elements, respectively.

This description of fracture as a change of element identity is consistent with the use of the the semi-grand canonical ensemble $(\Delta\mu, V, T)$, typically use in the study of binary mixtures and adsorption processes [13, 14]. Within this framework, two new descriptors emerge for the fracture problem: the chemical potential difference $\Delta\mu$, representing a radiation source, affecting equally each elements' transition to the fractured state, and the kinetic temperature T, quantifying the system disorder (i.e uncertainty).

In this framework, the number of elastic elements N_e can be described by the following functional equation:

$$N_e = \mathcal{F}(\Delta\mu, T, x), \tag{1}$$

where x stands for the prescribed loading. Recalling the surface nature of fracture processes, the previous formulation simplifies to:

$$N_e \approx \mathcal{F}(\Delta\mu, T) \tag{2}$$

This formulation parallels gas adsorption equilibria [15], where the volume of adsorbed particles (e.g elements in solid state) is driven by the adsorption pressure (here $\Delta\mu$) and the system temperature T. The optimal adsorption configuration at a fixed external loading may be found by minimizing the system's semi-grand potential Y, expressed as:

$$Y = F - \Delta\mu N_e \tag{3}$$

where F is the Helmholtz energy function. It remains to precise the form of F for the fracture problem. One suitable formulation is the extended deformation-fracture potential proposed by Francfort and Marigo [17], which encompasses both the deformation energy of the solid, and the fracture energy dissipated along fracture surfaces Γ:

$$U(\vec{x}, \Gamma) = \underbrace{\int_{\Omega/\Gamma} u_\lambda(\vec{x})\, \mathrm{d}V}_{U_\lambda} + \underbrace{\int_\Gamma \mathcal{G}_c\, \mathrm{d}S}_{U_\Gamma} \tag{4}$$

where U_λ stands for the potential energy due to deformation in the canonical ensemble; whereas U_Γ is the fracture energy, $\mathcal{G}_c$ that is dissipated in the creation of fracture surface, Γ. Originally introduced as an energy minimization problem for both the displacement field, and fracture surface, the potential expression (4) resembles formally Embedded-Atom Methods (EAM), in which the the total energy is the sum of pair-wise interactions due to particle distances and some embedding functions representative of the ground-state energy [18]; hence formally:

$$U(\vec{x}, N_b) = U_\lambda(\vec{x}) + \sum_{k=1}^{N_0} s^k \epsilon_0^{(k)} \tag{5}$$

where ϵ_0 is the groundstate energy released in the rupture of bond $i = 1...N_b$. The formal analogy between Eq. (4) and Eq. (5), allows us to link the fracture energy of brittle fracture to the groundstate energy:

$$\sum_{k=1}^{N_0} s^k \epsilon_0^{(k)} = \int_\Gamma \mathcal{G}_c \, \mathrm{d}S \tag{6}$$

In order to minimize the semi-grand potential Y we proceed by exploring fracture microstates and evaluating their likelihood by making use of Monte Carlo simulations. Given fixed mechanical boundary conditions (e.g. prescribed loads and displacements), we select an element at random and flip its fracture state $s^k = 1 - s^k$. Given a proposed fracture state transition from micro-state o to n, its acceptance is driven by the following criterion [16]:

$$acc(o \to n) = min(1, p_{o \to n}) \tag{7}$$

where $p_{o \to n}$, for an arbitrary fracture site k, is defined as:

$$\begin{cases} p_{o \to n} \overset{\text{fracture}}{=} \exp\left[\beta\left(-\Delta\mu - \Delta\mathcal{U}_{e(k) \to f(k)}\right)\right] \\ p_{o \to n} \overset{\text{healing}}{=} \exp\left[\beta\left(+\Delta\mu - \Delta\mathcal{U}_{b(k) \to e(k)}\right)\right] \end{cases} \tag{8}$$

Herein, $\Delta\mathcal{U}_{e(k) \to b(k)} = -\Delta\mathcal{U}_{b(k) \to e(k)} = \epsilon_0^k - U_\lambda^k$.

2.2 Extension to damage processes

Given the formulation of brittle fracture as a binary process, best described by mono-layer adsorption theory, it seems natural to extend this analogy to damage by describing it as a multilayer adsorption process. Considering a finite number of N_d admissible damage states and an associated $\vec{\omega} \in [0, 1]$, we can modify the fracture state variable presented in Section 2.1 into a damage state vector $\vec{s} = \sum_{i=1}^{N_d} \delta_{ji} \vec{e}_i$ so that:

$$\forall i = 1...N_0; \;\; \omega_i = \vec{s}^{(i)} \cdot \vec{\omega} \tag{9}$$

The transition between damage states is defined by a state transition matrix ($\mathbf{P}$) such that $\vec{s}_n^{(k)} = \mathbf{P}^T \cdot \vec{s}_o^{(k)}$. The elements of $\mathbf{P}$ define the conditional probability $P_{o,n} = \Pr(n \mid o)$ to transition from damage state $j = o$ to damage state $j = n$. Within the brittle fracture framework previously presented, state transitions can be expressed using a transition matrix $\mathbf{P}$ applied over the state vector $\vec{s}$, where $\mathbf{P}$ reads:

$$\mathbf{P} = \begin{bmatrix} 0 & 1 \\ 1 & 0 \end{bmatrix}.$$

For a system with N_d damage states, a logical choice to make in the structure of $\mathbf{P}$ is to consider unbiased transitions to adjacent damage states only. In other words, the transition matrix generalizes to:

$$\mathbf{P} = \begin{bmatrix} 0 & 1/2 & 0 & \dots & 0 & 0 & 0 \\ 1 & 0 & 1/2 & \dots & 0 & 0 & 0 \\ 0 & 1/2 & 0 & \dots & 0 & 0 & 0 \\ \vdots & \vdots & \vdots & \ddots & 1/2 & 0 & 0 \\ 0 & 0 & 0 & \dots & 0 & 1/2 & 0 \\ 0 & 0 & 0 & \dots & 1/2 & 0 & 1 \\ 0 & 0 & 0 & \dots & 0 & 1/2 & 0 \end{bmatrix}.$$

where the asymmetry in the transition proposal for the boundary states should be accounted for in the acceptance criterion.

A typical simplification in physics of compositional changes is to consider that the potential difference between adjacent states is independent of the state themselves. In other words, considering two arbitrary damage states $(i, i+1) \in \{1, ..., N_d - 1\}$ and their associated chemical potential (μ_i, μ_{i+1}):

$$\Delta\mu := \mu_{i+1} - \mu_i \tag{10}$$

The acceptance criterion for a damage transition $o \to n$ is then readily extended from Equation 8 as:

$$p_{o \to n} = \exp[-\beta(\Delta U - \delta \, \Delta\mu)] \leq 1 \tag{11}$$

where $\delta = \text{sign}(\omega_n^{(k)} - \omega_o^{(k)}) = \pm 1$ indicates the direction of the damage progression and the exact form ΔU will be further discussed in Section 3.2.

Finally, it is worth highlighting that the damage state vector $\vec{s}$ and the associated $\vec{\omega}$ provide a measure of material performance through the

(undamaged) bond "mass" density ρ, analogous to the number of solid elements N_e in a binary fracture process. This relationship is expressed as:

$$\rho = 1 - \frac{1}{N_0}\sum_{k=1}^{N_0} \vec{s}^{(k)} \cdot \vec{\omega} \tag{12}$$

This formulation allows us to draw a formal parallel between ρ and the equivalent monolayer thickness θ in adsorption physics [15], which quantifies the average number of layers deposited on the adsorbent—essentially representing the system's average remaining performance. In this analogy, damage can naturally be described using the framework of multi-layer adsorption physics, where a fixed number N_d of adsorption layers is considered.

3 IMPLEMENTATION

3.1 Reduced Units

Our simulation-based investigation is carried out in reduced units (or Lennard Jones units, see [16]), commonly employed in molecular simulations for purpose of scaling. Reduced units originate from a dimensional analysis of all quantities using as set of dimensionally independent quantities a reference groundstate energy, ϵ_0 and a reference distance between particles, D, typically associated with a bond equilibrium distance. Derived quantities are the reduced temperature, $T^* = k_B T/\epsilon_0 = (\beta\epsilon_0)^{-1}$; and mechanical quantities, such as forces, $\vec{F}^* = \vec{F}(D\epsilon_0^{-1})$, moments $\vec{M}^* = \vec{M}(\epsilon_0^{-1})$, stresses $\sigma^* = \sigma(D^3\epsilon_0^{-1})$. To generalize this system of reduced units to $d = 2$ and $d = 3$ dimensions, it is useful to introduce two length dimensions for in-plane (D_R) and out-of-plane (D_z) length dimensions, and scale the elastic moduli (K^*, G^*, κ^*), the fracture energy ($\mathcal{G}_c^*$) and the fracture toughness ($\mathcal{K}_c^* \sim \sqrt{G^*\mathcal{G}_c^*}$) as,

$$(K^*, G^*, \kappa^*) = (K, G, \kappa)\left(\frac{D_R^d D_z^{3-d}}{\epsilon_0}\right) \tag{13}$$

$$\mathcal{G}_c^* = \mathcal{G}_c\left(\frac{D_R^{d-1} D_z^{3-d}}{\epsilon_0}\right) \tag{14}$$

$$\mathcal{K}_c^* = \mathcal{K}_c\left(\frac{D_R^{d-1/2} D_z^{3-d}}{\epsilon_0}\right) \tag{15}$$

where κ will be defined in Section 3.2. These scaling relations highlight the extensive nature of the groundstate energy (ϵ_0), in contrast to the intensive nature of Griffith's fracture energy ($\mathcal{G}_c$). We keep these scaling relation in mind in forthcoming applications.

3.2 Short-Range and Long-Rang Continuum-Based Interaction Potentials

One feature, which distinguishes our approach from previous fluctuation-based fracture developments [19–21], is the consideration of bond interaction potentials using continuum-based finite elements. In the continuum approach, short-range interactions are taken into account by classical elastic constitutive equations in function of the displacement gradient, $\boldsymbol{\zeta} = \nabla\vec{x}$. For instance, for an isotropic material in the harmonic limit:

$$U_\lambda^{(k)} = \frac{1-\omega^{(k)}}{2}\int_{\mathcal{P}_k} [K\,\varepsilon_v^2 + 2G\,(\boldsymbol{\varepsilon} : \boldsymbol{\varepsilon} - \frac{1}{3}\varepsilon_v^2)]\,\mathrm{d}V \tag{16}$$

where K, G stand for bulk and shear modulus; $\boldsymbol{\varepsilon} = \frac{1}{2}(\zeta + \zeta^T)$ is the symmetric strain tensor; and $\varepsilon^v = \mathrm{tr}\,\boldsymbol{\zeta} = \nabla \cdot \vec{x}$ is the volume strain. Expression (16) is the continuum counterpart of 2-pt interactions based upon the distance between particles. Implemented in the finite element method, the displacement gradient is approximated by $\boldsymbol{\zeta} = [B_{ij}](x)_j$, with $[B_{ij}]$ the strain-displacement matrix, and $(x)_j$ the vector of nodal displacements of the element [22].

Furthermore, in our investigation we consider also long-range interactions in form of the recently proposed sprain theory [23–25]: an enriched potential formulation considering curvature effects in form of the gradient of the dis-

placement gradient, $\nabla\boldsymbol{\zeta} = \nabla(\nabla\vec{x})$:

$$U_\chi^{(k)} = \frac{f(\omega_k)}{2}\int_{\mathcal{P}_k} \kappa\left(\ell_0\nabla\boldsymbol{\zeta}\right)^2 \mathrm{d}V \qquad (17)$$

where κ is the curvature modulus, while ℓ_0 is a material length scale over which the long-range curvature effects are activated. Finally, these long-range interactions can be modulated by a function f, which is dependent on local damage. In this paper, we will restrict ourselves to two forms of f, $f(\omega_k) = 1$ considering curvature interactions to be independent of damage, as presented in [23], and $f(\omega_k) = H(1-\omega^k)$ where long-range interations cease at complete damage.

Expression (18) can be viewed as the continuum counter-part of 3-pt and 4-pt interactions that generate a restoring energy due to angle variations, represented –in the continuum setting– by the curvature $\nabla\boldsymbol{\zeta}$. Finally, for the finite element implementation of the long-range interactions, we use the recently proposed Lagrange multiplier constraint, which enforces an approximate displacement gradient constraint, $\boldsymbol{\zeta} - \nabla\vec{x} \to 0$, over each element, without altering the energy density due to curvature effect; that is [23, 25]:

$$U_\chi^{(k)} = \frac{f(\omega_k)}{2}\int_{\mathcal{P}_k} \left[\kappa\left(\ell_0\nabla\boldsymbol{\zeta}\right)^2 + \boldsymbol{\Lambda} : \left(\boldsymbol{\zeta} - \nabla\vec{x}\right)\right] \mathrm{d}V \qquad (18)$$

with $\boldsymbol{\Lambda}$ the Lagrange multipliers, which are unknowns of the deformation energy minimization problem at fixed damage state.

4 APPLICATIONS

In this section, we analyze the outputs of our fluctuation-based fracture method, focusing on a notched beam subjected to a three-point bending test. Specifically, we investigate the three models previously described: linear elastic fracture mechanics (LEFM), local continuum damage (CDM), and sprain theory with the f-function formulation introduced in Section 3.2. For this analysis, we consider a reduced material length $l_0^* = 2$ and $\kappa^* = E^*/15$, as suggested in [23].

5 Fracture Micro-States

We first conduct a classical displacement-driven load test on the notched beam under $\Delta\mu^* = 0$, assuming a homogeneous ground-state energy ϵ_0^*. At low kinetic temperatures ($T^* = 10^{-5}$, *Fig.* 1B.), the fracture process zone in the CDM sample is confined to a narrow band, with damage localizing within a single element. Complete failure occurs before any propagation of micro-defects beyond the crack tip. Consequently, quasi-brittle fracture cannot be characterized by similarity laws [26]; the solution remains mesh-dependent, and in the thermodynamic limit ($N_0 \to \infty$), energy dissipation vanishes.

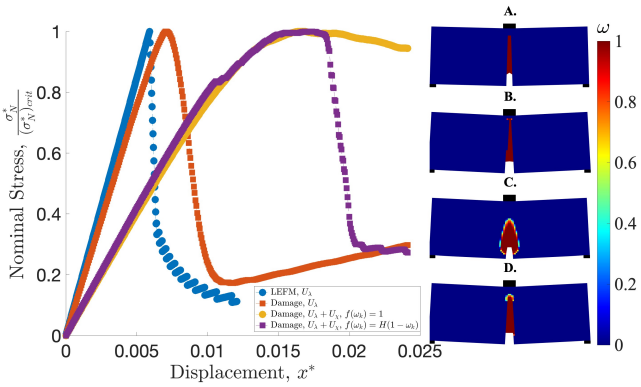

Figure 1: Normalized nominal stress as a function of imposed displacement at low kinetic temperature ($T^* = 10^{-5}$). The equilibrium damage micro-state at maximum displacement (x^*) is shown for: A) local (LEFM) interactions, B) local (damage) interactions, and curvature-enriched interactions that are C) constant with respect to damage ($f(\omega_k) = 1$), and D) vanishing at maximum damage ($f(\omega_k) = H(1-\omega_k)$).

Here, damage functions primarily as a continuous approximation of LEFM, which inherently comprises two equilibrium states (*Fig.* 1A). Unlike LEFM (*Figs.* 1A and 2A), no temperature-induced transition from directed fracture to random nucleation is observed in damage models (*Figs.* 2B, 2C, and 2D). Even at high kinetic temperatures ($T^* = 1$), kinetic agitation enables the emergence of a distinct fracture pattern. The significant number of adsorption layers ($N_d \geq 500$) mitigates temperature effects, confining random material degradation

to the initial damage layers. Thermodynamically, the accessibility of intermediate damage states is achievable only by incorporating long-range interactions into the damage formulation (*Figs.* 1C and 1D). This non-local energy redistribution introduces a restoring force that maintains cohesion, explaining the delayed onset of damage when the enhanced energy term $U = U_\lambda + U_\chi$ is considered (*Fig.* 1).

However, it is important to note that making these long-range interactions independent of damage ($f(\omega_k) = 1$) can result in spurious lateral damage spread (*Fig.* 1C) and an extended damage tail due to the constant restoring force. Consequently, for the remainder of this study, we focus on curvature-enriched interactions modulated by the function $f(\omega_k) = H(1-\omega_k)$.

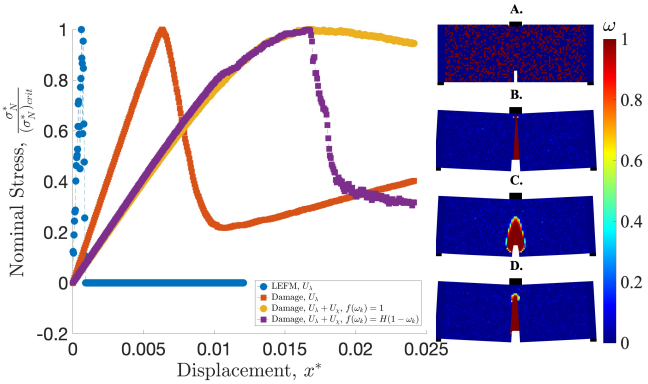

Figure 2: Normalized nominal stress as a function of imposed displacement at high kinetic temperature ($T^* = 1$). The equilibrium damage micro-state at maximum displacement (x^*) is shown for: A) local (LEFM) interactions, B) local (damage) interactions, and curvature-enriched interactions that are C) constant with respect to damage ($f(\omega_k) = 1$), and D) vanishing at maximum damage ($f(\omega_k) = H(1-\omega_k)$).

5.1 Isosteric Heats of Adsorption

In this section, we establish a statistical analogue to Griffith's fracture criterion [1] using isosteric heats of adsorption, as first proposed in [21]. Within the framework of LEFM, we define the elastic heat of adsorption—analogous to the elastic energy release rate—as follows [27]:

$$q_\lambda^* = -\frac{\partial\langle U_\lambda^*\rangle}{\partial\langle N_f\rangle} = -\frac{\mathrm{cov}(U_\lambda^*, N_f)}{\mathrm{var}(N_f)} = \frac{\partial\langle U_\lambda^*\rangle}{\partial\langle N_e\rangle}. \tag{19}$$

Similarly, by defining $U_0^* = \sum_{k=1}^{N_0} s^k(\epsilon_0^{(k)})^*$, the critical isosteric heat of adsorption is expressed as:

$$q_0^* = \frac{\partial\langle U_0^*\rangle}{\partial\langle N_e\rangle} \underset{\text{sample}}{\overset{\text{Hom.}}{=}} 1. \tag{20}$$

This ensemble-based formulation circumvents the need for experimental determination of the critical energy release rate, traditionally performed via size-effect studies [28], and eliminates complexities associated with numerical derivatives [29, 30]. For multi-layer adsorption processes, the extension is straightforward by replacing the number of elastic elements with the undamaged bond mass density ρ:

$$\begin{cases} q_\lambda^* = \dfrac{1}{N_0}\dfrac{\partial\langle U_\lambda^*\rangle}{\partial\langle\rho\rangle}, \\ q_0^* = \dfrac{1}{N_0}\dfrac{\partial\langle U_0^*\rangle}{\partial\langle\rho\rangle}. \end{cases} \tag{21}$$

From an adsorption perspective, variations are observed with respect to the equivalent adsorbed monolayer thickness.

As shown in *Fig.* 3, the limit energy release rate consistently converges to a singular value, regardless of the system's kinetic temperature, thereby reinforcing its role as a marker for directed fracture propagation. Notably, $q_0^* = 1$ arises naturally from our use of reduced units, as demonstrated in *Eq.* (20).

Examining the elastic heat of adsorption q_λ^*, two distinct regimes emerge at low kinetic temperatures ($T^* < 10^{-1}$). For LEFM and local CDM, there is an initial overshoot of the critical energy release rate q_0^* at damage initiation. In the LEFM context (*Fig.* 3a), this overshoot highlights the instability of LEFM due to its two-state formulation, violating Griffith's criterion. Conversely, in the CDM context (*Fig.* 3b), q_λ^* quantifies energy dissipation due to damage, where $q_\lambda^* > q_0^*$ for $x^* \in [0.007, 0.012]$, corresponding to the global instability regime seen

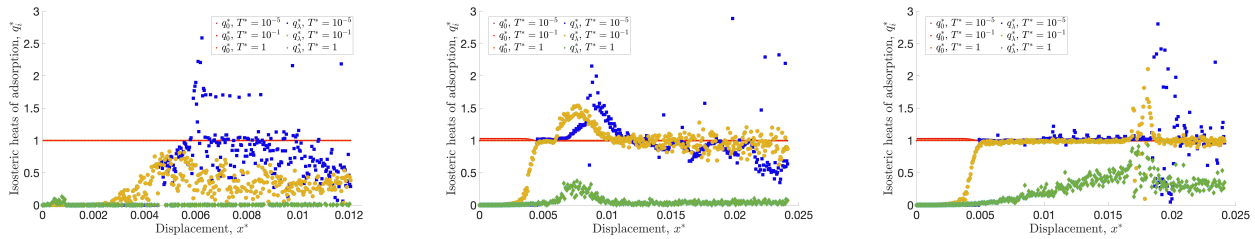

Figure 3: Isosteric heats of adsorption. (a) The LEFM criterion relies on the elastic configurational volume N_e, while (b) CDM and (c) Sprain models utilize the undamaged bond density ρ.

in the σ_N^* plot of *Fig.* 1. This behavior mirrors dynamic fracture mechanics, where the crack velocity balances the elastic energy release rate with its critical counterpart. In local damage models, the absence of energy redistribution across a defined fracture width triggers additional damage at the crack tip, transitioning the fracture process from quasi-static to dynamic and challenging the treatment of damage as a thermodynamic process at equilibrium. However, long-range interactions (*Fig.* 3c) facilitate energy redistribution, mitigating crack velocities and stabilizing the process. Here, $q_\lambda^* = q_0^*$ almost everywhere after damage initiates, with minor instabilities around $x^* \approx 0.017$, corresponding to global instability onset (*Fig.* 1).

Additionally, heat of adsorption observables serve as valuable indicators to differentiate among various failure regimes, contrarily to damage micro-states (*Fig.* 2).Even though large kinetic temperatures allow the emergence of directed cracks in the case of (non)-local damage models, the underlying fracture mechanism can be resolved by analyzing our statistical Griffith's criterion. Notably, a transition temperature $T^* \in [0.1, 1]$ exists where $q_\lambda^* < q_0^*$ for all damage states d^* and the system becomes nucleation-driven. The magnitude of q_λ^* at high temperature in *Fig.* 3c suggests that the presence long-range interactions increases the transition temperature, due to their associated restoring force.

5.2 Damage Isotherms

The classical fracture framework is extended by testing the notched beam under a non-zero chemical potential difference, $\Delta\mu^*$. This $\Delta\mu^*$ acts as a configurational pressure difference, modifying the ground-state energy of the reference sample to an effective ground-state energy, $\tilde{\epsilon}_0^* = \epsilon_0^* + \Delta\mu^*$. This modification uniformly affects each adsorption layer in multilayer scenarios. Using this framework, we construct damage isotherms that quantify the configurational adsorbed volume as a function of $\Delta\mu^*$ at a fixed load (*Fig.* 4).

For LEFM, two distinct regimes are observed (*Fig.* 4a). At low temperatures ($T^* = 10^{-5}$), the adsorbed volume remains largely unaffected by $\Delta\mu^*$ until a zero dissipation potential is reached ($\Delta\mu^* = -1$), where the adsorbed volume drops sharply to zero. This behavior indicates the dominance of directed fracture as the primary failure mechanism across the range of permissible chemical potential differences.

At higher temperatures ($T^* = 1$), the isotherms display a linear correlation between the adsorbed volume and configurational pressure, converging to $1/2$ before complete desorption occurs at $\Delta\mu^* = -1$. This behavior suggests a transition to random nucleation as the dominant mechanism. For intermediate temperatures ($T^* \approx 0.1$), gradual desorption begins around $\Delta\mu^* \approx -1/2$, with notable inflection points near $\Delta\mu^* = -0.8$, indicative of material reorganization. These behaviors are consistent with Type I isotherms characterized by an infinite Henry's constant [15], reflecting the two-state nature of LEFM systems.

The damage model isotherms (*Fig.* 4b) further support the interpretation of CDM as an extension of LEFM. At low kinetic temperatures ($T^* = 10^{-5}$), the damage isotherms exhibit behavior similar to their LEFM counter-

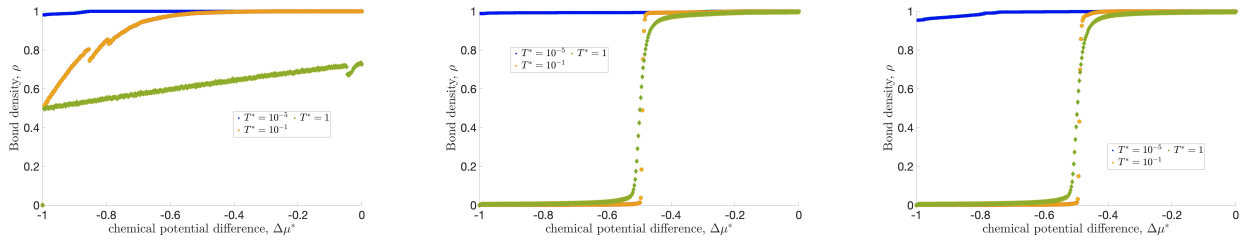

Figure 4: Damage isotherms $(\rho, \Delta\mu^*)$ measured at fixed loading for $T^* \in [10^{-5}, 1]$. a) LEFM isotherms; b) Local CDM: the configurational volume is equivalent to the monolayer thickness; c) Non-local CDM: fracture width influences the desorption response.

parts, including an infinite Henry's constant and a sharp transition from fracture-driven desorption to complete volume desorption at $\Delta\mu^* = -1$. In contrast, the inclusion of long-range interactions (*Fig.* 4c) introduces progressive material desorption, highlighting the accessibility of intermediate damage states.

At higher temperatures ($T^* \geq 0.1$), a transition from Type I to Type V is observed, irrespective of the presence of long-range interactions indicating multi-layer adsorption and capillary condensation phenomena [31](*Figs.* 4b and 4c).

6 CONCLUSIONS

This study introduces a statistical mechanics framework for analyzing fracture and damage processes in concrete materials, leveraging the semi-grand canonical ensemble. By treating fracture as a monolayer adsorption process and damage as a multi-layer adsorption phenomenon, we have successfully linked classical fracture energy concepts to statistical observables. The incorporation of long-range interactions, as captured by curvature-enriched potentials, proved pivotal in stabilizing damage propagation and allowing accessibility to intermediate damage states.

Key findings include the ability of statistical observables, such as isosteric heats of adsorption, to provide insights into failure mechanisms, effectively differentiating between regimes dominated by directed fracture or random nucleation. Damage isotherms highlighted the influence of configurational pressure on material degradation, confirming transitions between fracture and gas-like desorption at various kinetic temperatures. Notably, the statistical extension of Griffith's criterion enables a more nuanced understanding of energy dissipation, readily available as an output of our framework.

Looking ahead, the ability to manipulate the chemical potential difference $\Delta\mu^*$ to modify the ground-state energy presents a promising direction for future research. This extension would enable the modeling of fracture phenomena driven by energy variations, such as size effects. By refining the predictive power of this approach, the framework can be applied to a broader range of quasi-brittle and heterogeneous materials, advancing the understanding of fracture mechanics across diverse contexts.

REFERENCES

[1] Griffith, A. A., Taylor, G.I. 1921. The phenomena of rupture and flow in solids. *Philosophical Transactions of the Royal Society of London. Series A, Containing Papers of a Mathematical or Physical Character*; pp. 163-198.

[2] Nuismer, R.J., 1975. An energy release rate criterion for mixed mode fracture. *International journal of fracture*; pp.245-250.

[3] Toya, M., 1992. On mode I and mode II energy release rates of an interface crack. *International journal of fracture*; pp.345-352.

[4] Hayashi, K, Nemat-Nasser, S., 1981. Energy-release rate and crack kinking un-

der combined loading. *Journal of Applied Mechanics*; pp. 520-524

[5] Sih, G. C, Paris, P. C., Irwin, G. R. 1965. On cracks in rectilinearly anisotropic bodies. *International Journal of Fracture Mechanics*; pp. 189-203.

[6] Bourdin, B., Francfort, G.A., Marigo, J.J., 2008. The variational approach to fracture. *Journal of elasticity*; pp.5-148.

[7] Schmidt, B., Fraternali, F., Ortiz, M., 2009. Eigenfracture: an eigendeformation approach to variational fracture. *Multiscale Modeling & Simulation*; pp. 1237-1266.

[8] Miehe, C., Hofacker, M., Welschinger, F., 2010. A phase field model for rate-independent crack propagation: Robust algorithmic implementation based on operator splits. *Computer Methods in Applied Mechanics and Engineering*; pp. 2765-2778.

[9] Zhang, X., Sloan, S.W., Vignes, C., Sheng, D., 2017. A modification of the phase-field model for mixed mode crack propagation in rock-like materials. *Computer Methods in Applied Mechanics and Engineering*; pp.123-136.

[10] Zhou, S., Zhuang, X., Zhu, H., Rabczuk, T., 2018. Phase field modelling of crack propagation, branching and coalescence in rocks. *Theoretical and Applied Fracture Mechanics*; pp.174-192.

[11] Yin, B.B., Zhang, L.W., 2019. Phase field method for simulating the brittle fracture of fiber reinforced composites. *Engineering Fracture Mechanics*; pp.321-340.

[12] Bažant, Z.P., and Pfeiffer, P.A., 1987. Determination of fracture energy from size effect and brittleness number. *ACI Materials Journal*; pp. 463-480.

[13] Ramalingam, H., Asta, M., Van de Walle, A., Hoyt, J.J., 2002. Atomic-scale simulation study of equilibrium solute adsorption at alloy solid-liquid interfaces. *Interface science*; pp.149-158.

[14] Kofke, D.A., Glandt, E.D., 1988. Monte Carlo simulation of multicomponent equilibria in a semigrand canonical ensemble. *Molecular Physics*; pp.1105-1131.

[15] Tien C., 2018. *Introduction to adsorption: Basics, analysis, and applications*; Elsevier.

[16] Frenkel, D., Smit, B., 2023. *Understanding molecular simulation: from algorithms to applications*; Elsevier.

[17] Francfort, G.A., Marigo, J.J., 1998. Revisiting brittle fracture as an energy minimization problem. *Journal of the Mechanics and Physics of Solids*; pp.1319-1342.

[18] Daw, M.S. and Baskes, M.I., 1984. Embedded-atom method: Derivation and application to impurities, surfaces, and other defects in metals. *Physical Review B*, p.6443.

[19] Mulla, T., Pellenq, R.M. and Ulm, F.J., 2022. Fluctuation-based fracture mechanics of heterogeneous materials. *Physical Review E*, 106(6), p.065003.

[20] Mulla, T., Moeini, S., Ioannidou, K., Pellenq, R.M. and Ulm, F.J., 2021. Phase diagram of brittle fracture in the semi-grand-canonical ensemble. *Physical Review E*, 103(1), p.013003.

[21] Al-Mulla, T., Pellenq, R.J.M. and Ulm, F.J., 2018. Griffith's postulate: Grand canonical Monte Carlo approach for fracture mechanics of solids. *Engineering Fracture Mechanics*, 199, pp.544-554.

[22] Bathe, K.J., 2006. *Finite element procedures*. Klaus-Jurgen Bathe.

[23] Nguyen, A.T., Xu, H., Matous, K. and Bazant, Z.P., 2023. Smooth Lagrangian Crack Band Model (slCBM) Based on Spress-Sprain Relation and Lagrange Multiplier Constraint of Displacement Gradient. *Journal of Applied Mechanics*, pp.1-19

[24] Zhang, Y. and Bažant, Z.P., 2023. Smooth crack band model—A computational paragon based on unorthodox continuum homogenization. *Journal of Applied Mechanics*, 90(4), p.041007.

[25] Xu, H., Nguyen, A.T. and Bažant, Z.P., 2024. Sprain energy consequences for damage localization and fracture mechanics. *Proceedings of the National Academy of Sciences*, 121(40), p.e2410668121.

[26] Barenblatt, G.I., 1996. *Scaling, self-similarity, and intermediate asymptotics: dimensional analysis and intermediate asymptotics* (No. 14). Cambridge University Press.

[27] Nicholson, D. and Parsonage, N.G., 1982. *Computer simulation and the statistical mechanics of adsorption*.

[28] Bazant, Z.P. and Pfeiffer, P.A., 1987. Determination of fracture energy from size effect and brittleness number. *ACI Materials Journal*, 84(6), pp.463-480.

[29] Zehnder, A.T., 2012. *Fracture mechanics* (Vol. 62). Springer Science & Business Media.

[30] Nagashima, T., Omoto, Y. and Tani, S., 2003. Stress intensity factor analysis of interface cracks using X-FEM. *International Journal for Numerical Methods in Engineering*, 56(8), pp.1151-1173.

[31] Donohue, M.D. and Aranovich, G.L., 1998. Classification of Gibbs adsorption isotherms. *Advances in colloid and interface science*, 76, pp.137-152.